

# **The non-self-adjoint thin film problem: dynamics of fixed-volume pinned films**

Israel Gabay<sup>1</sup>, Vesna Bacheva<sup>2</sup>, Dotan Ilssar<sup>3</sup>, Moran Bercovici<sup>1\*</sup>, Antonio Ramos<sup>4</sup>, Amir Gat<sup>1\*</sup>

<sup>1</sup>*Faculty of Mechanical Engineering, Technion – Israel Institute of Technology, Haifa, Israel*

<sup>2</sup>*IBM Research Europe, Zurich, Switzerland*

<sup>3</sup>*Department of Mechanical and Process Engineering, ETH Zürich, Zürich 8092, Switzerland*

<sup>4</sup>*Depto. Electronica y Electromagnetismo, Facultad de Fisica, Universidad de Sevilla, Sevilla, Spain*

*\*corresponding authors: M.B. ([mberco@technion.ac.il](mailto:mberco@technion.ac.il)) and A.G ([amirgat@technion.ac.il](mailto:amirgat@technion.ac.il))*

## **ABSTRACT**

Existing solutions for film dynamics fail when considering the most standard and straightforward implementation – a pinned film in an impermeable domain, such as used in liquid actuators or adaptive optical elements. We present a solution methodology to the linearized non-self-adjoint system that arises from this problem, and validate it experimentally using holographic measurements of a liquid film subjected to a desired normal force distribution through dielectrophoresis. The study shows that confined films exhibit fundamentally different behavior than that predicted by existing models.

## Introduction

The deformation of thin liquid films has been investigated for more than a century [1,2], owing to their importance in a wide range of natural phenomena [3–7] and engineering applications [8–11]. To date, solutions to the thin film problem have focused solely on boundary conditions describing infinite films [12,13], periodic films [14–16], or those that give rise to self-similar solutions [9,10,17,18]. Surprisingly, despite the fact that a large number of applications and phenomena involve films that are pinned on impermeable boundaries, analytical modeling of this fundamental case has been overlooked. While existing solutions provide general insight into thin films dynamics, the non-penetration conditions at the boundaries of finite domains, together with pinning conditions, eliminate the self-adjointness of the governing equations, and drive dynamics that are substantially different.

Among the engineering applications of thin films in close domains, one of the most active fields of research is adaptive optics where interfacial deformations can be leveraged to create smooth optical elements [19–22]. Another emerging application is in the field of reconfigurable microfluidics [23], where thin liquid films could be used to dynamically deform the surface of a thin membrane of a microfluidic chip, in order to control its functionality in real time. The film dynamics in such applications can be described by the same set of equations, whether a liquid-fluid or a liquid-membrane interface is used [24–27]. The ability to design such devices, predict their performance, and understand their fundamental limitations, would greatly benefit from a theoretical framework that allows their analysis.

We here present a combined theoretical and experimental study of the dynamics of a thin liquid film that is pinned on the boundaries of an impermeable finite domain, and subjected to a normal stress distribution at its liquid-air interface. We provide a time-dependent closed-form analytical solution for the linearized evolution problem, which is non-self-adjoint. We compare these solutions with the existing solutions for the same configuration but with self-adjoint boundary conditions, and show that while the initial dynamics are identical, the difference in boundary conditions quickly affects the entire domain, resulting in significant differences between the two. To experimentally illustrate the dynamics and to validate the model, we developed a setup that enables high frame-rate measurements of microscale deformations based on digital holography. We use this setup to investigate the deformation of a thin liquid film actuated by an array of electrodes imposing a dielectrophoretic (DEP) force on the interface [28], showing good agreement to the theory.

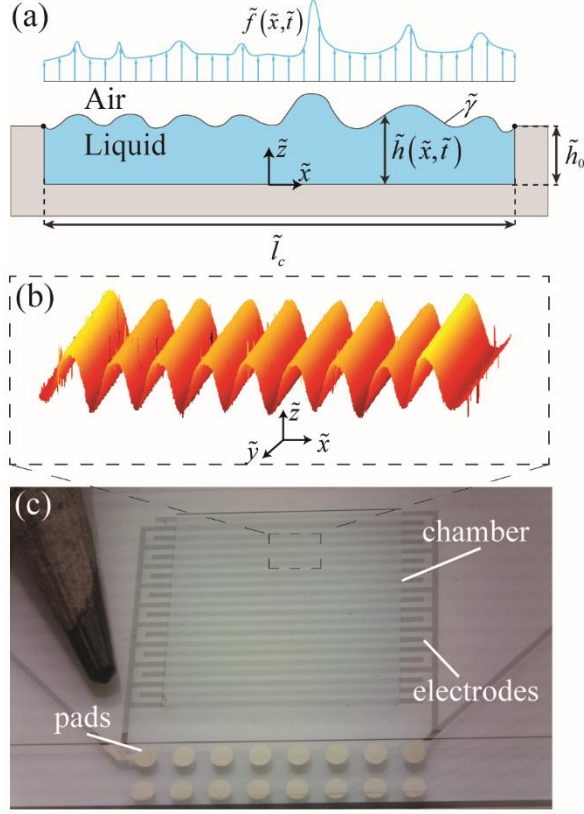


FIG. 1. (a) Two-dimensional illustration of the investigated model comprised of a shallow chamber of length  $\tilde{l}_c$  and height  $\tilde{h}_0$  filled with a liquid of mass density  $\tilde{\rho}$ , dynamic viscosity  $\tilde{\mu}$ , and open to the air above. The liquid-air interface with surface tension  $\tilde{\gamma}$  is subjected to a normal force distribution  $\tilde{f}(\tilde{x}, \tilde{t})$ , resulting in a deformed liquid height  $\tilde{h}(\tilde{x}, \tilde{t})$ . At the edges of the chamber the liquid is pinned and cannot penetrate the solid, resulting in global mass conservation. (b) Example of an experimentally observed deformation of the liquid film when subjected to a DEP force distribution. (c) Image of the microfabricated chamber used in the experiments. The bottom of the chamber is patterned with an array of electrodes imposing a dielectrophoretic (DEP) force on the interface.

*Analytical model.* Figure 1 presents an illustration of the investigated configuration. Consider a shallow chamber of depth  $\tilde{h}_0$  and length  $\tilde{l}_c$  filled with a Newtonian liquid of mass density  $\tilde{\rho}$ , dynamic viscosity  $\tilde{\mu}$  and volume  $\tilde{V}$ . The liquid-air interface has a surface tension  $\tilde{\gamma}$  and is subjected to a normal force distribution  $\tilde{f}(\tilde{x}, \tilde{t})$  that induces a spatio-temporal deformation of the interface,  $\tilde{h}(\tilde{x}, \tilde{t})$ . A full derivation of the governing equations is provided in the Supplemental Material [29]. Briefly, under the assumptions of a shallow geometry ( $\tilde{h}_0 \ll \tilde{l}_c$ ), negligible fluid inertia, and requiring no-slip at the bottom surface and a stress-balance at the free surface [8,30], the Navier-Stokes equations can be simplified to

$$(0.1) \quad \frac{\partial \tilde{h}}{\partial \tilde{t}} = \frac{1}{3\tilde{\mu}} \frac{\partial}{\partial \tilde{x}} \left( \tilde{h}^3 \frac{\partial \tilde{p}}{\partial \tilde{x}} \right),$$

and

$$(0.2) \quad \tilde{p} = \tilde{\rho}\tilde{g}(\tilde{h} - \tilde{z}) - \tilde{\gamma} \frac{\partial^2 \tilde{h}}{\partial \tilde{x}^2} - \tilde{f},$$

where (1.1) is the evolution equation, and (1.2) is the fluidic pressure.

Denoting the film deformation as  $\tilde{d}(\tilde{x}, \tilde{t}) = \tilde{h}(\tilde{x}, \tilde{t}) - \tilde{h}_0$ , defining the following non-dimensional parameters  $\tilde{t} = t\tilde{\tau}$ ,  $\tilde{x} = x\frac{\tilde{l}}{2}$ ,  $\tilde{d} = d\tilde{h}_0$ ,  $\tilde{f} = \tilde{F}f$ , and assuming small deformations  $d \ll 1$ , we obtain the non-dimensional linearized evolution equation for the deformation,

$$(0.3) \quad \frac{\partial d}{\partial t} + \frac{\partial^4 d}{\partial x^4} - \text{Bo} \frac{\partial^2 d}{\partial x^2} = -\Pi \frac{\partial^2 f}{\partial x^2},$$

where  $\text{Bo} = \frac{\tilde{\rho}\tilde{g}\tilde{l}^2}{4\tilde{\gamma}}$  is the Bond number,  $\Pi = \frac{\tilde{F}\tilde{l}^2}{4\tilde{\gamma}\tilde{h}_0}$  represents the non-dimensional interfacial force

magnitude, and the resulting time scale is  $\tilde{\tau} = \frac{3\tilde{\mu}\tilde{l}^4}{16\tilde{h}_0^3\tilde{\gamma}}$ .

At the boundaries we require the liquid to be pinned,

$$(0.4) \quad d(x = \pm 1, t) = 0$$

and no penetration through the boundary, i.e.,  $u = 0$ . The latter requirement, under the lubrication approximation, yields  $\partial p / \partial x = 0$ . Applying this requirement to equation (0.2), yields the following boundary condition on the deformation,

$$(0.5) \quad \frac{\partial^3 d}{\partial x^3}(x = \pm 1, t) - \text{Bo} \frac{\partial d}{\partial x}(x = \pm 1, t) = -\Pi \frac{\partial f}{\partial x}(x = \pm 1, t).$$

These boundary conditions are accompanied by an initial condition,  $d_i = d(x, t = 0)$ .

The boundary conditions generate a non-self-adjoint system. To observe this, we first homogenize the boundary conditions by expressing the deformation as  $d(x, t) = \hat{d}(x, t) + P(x)\theta(t)$ , where  $P(x)$  is a polynomial function that is determined according to the force distribution at the boundaries [29]. To fully define the system, we assume that the force at the interface applied instantaneously upon activation of the electric field, and thus

$$(0.6) \quad \hat{d}_t + \hat{d}_{xxxx} - \text{Bo}\hat{d}_{xx} = -\Pi\theta(t)f_{xx} - P\delta(t) + \text{Bo}P_{xx}(x)\theta(t),$$

where  $\theta(t)$  is the Heaviside function,  $\delta(t)$  is the Dirac delta function and the corresponding boundary and initial conditions are,

$$(0.7) \quad \begin{aligned} \hat{d}(x = \pm 1, t) &= 0 \\ \frac{\partial^3 \hat{d}}{\partial x^3}(x = \pm 1, t) - \text{Bo} \frac{\partial \hat{d}}{\partial x}(x = \pm 1, t) &= 0. \\ \hat{d}(x, t = 0) &= d_i \end{aligned}$$

Next, taking the standard separation of variables approach, we suggest a solution of the form

$$(0.8) \quad \hat{d}(x, t) = \sum_{n=0}^{\infty} X_n(x)T_n(t).$$

We solve equation (0.6) by seeking a homogenous solution and using it to construct a particular one. The homogenous equation yields an eigenvalue problem,

$$(0.9) \quad -\frac{T'}{T} = \frac{X^{(4)}}{X} - \text{Bo} \frac{X''}{X} = \lambda_n^4,$$

which should be solved under the following boundary conditions,

$$(0.10) \quad X(\pm 1) = 0, \quad X'''(\pm 1) - \text{Bo}X'(\pm 1) = 0.$$

Since the spatial differential operator of equation (0.9),  $L$ , has constant real coefficients and only even derivatives, we are guaranteed that the Lagrange adjoint operator,  $L^+$  is identical to  $L$  [31]. To find the corresponding adjoint boundary conditions we require  $\langle L[X], Y \rangle = \langle X, L^+[Y] \rangle$ , where  $\langle U, V \rangle = \int_{-1}^1 U V dx$  is the basic inner product. Applying this inner product while integrating in parts and using the boundary conditions (0.10), yields

$$(0.11) \quad [X''Y' + X'Y'']_{-1}^1 = 0.$$

$Y$  is the solution of the adjoint problem, and its boundary conditions are defined such that equation (0.11) will hold. The boundary conditions of  $X$  are given by (0.10), and clearly if  $Y$  were to have the same boundary conditions, equation (0.11) would not hold. Thus, the problem is not self-adjoint. Equation (0.11) can be satisfied by the complementary boundary conditions  $Y'(\pm 1) = Y''(\pm 1) = 0$ , furnishing the adjoint system,

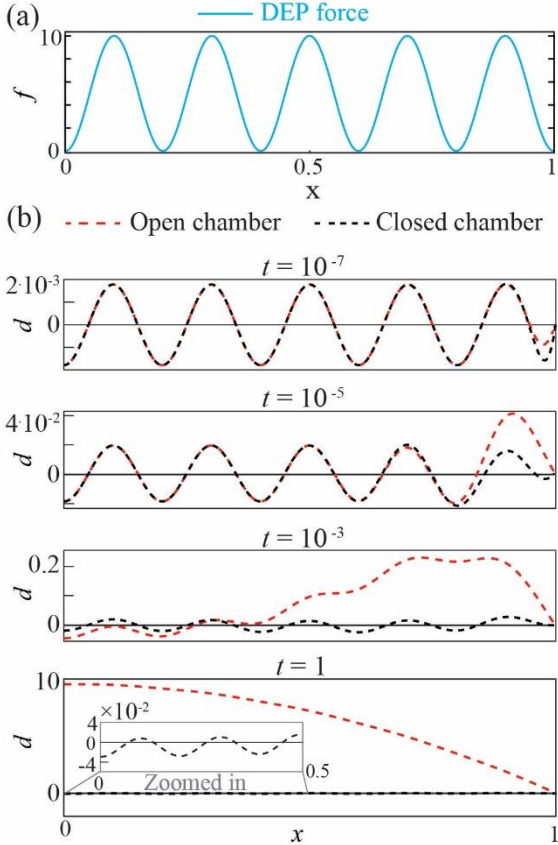
$$(0.12) \quad \begin{aligned} \frac{Y^{(4)}}{Y} - \text{Bo} \frac{Y''}{Y} &= \lambda_n^4 \\ Y'(\pm 1) &= Y''(\pm 1) = 0 \end{aligned}$$

The complete solution is provided in the Supplemental Material [29]. Briefly, the solution of equation (0.6) can now be obtained by finding the eigenvalues and eigenfunctions of each of the systems (original and adjoint), and by casting the RHS of the equation, and the initial condition in terms of the system's eigenfunctions. This is achieved by generalized Fourier series based on the system eigenfunctions. However, for the case of a non-self-adjoint system, the eigenfunctions of the original system are not orthogonal to themselves but rather to the adjoint eigenfunctions. Thus, for a general function  $g(x)$ , the coefficients  $c_n$  of the generalized Fourier series,  $g(x) = \sum_{n=0}^{\infty} c_n X_n(x)$  are found through orthogonality

$$\text{of } X_n \text{ with } Y_m \text{ for } n \neq m, \quad c_n = \frac{\int_{-1}^1 g(x) Y_n dx}{\int_{-1}^1 X_n Y_n dx}.$$

Figure 2 presents the solution for the deformation at different times for an initially flat interface subjected to a periodic force,  $f = 1 - \cos(10\pi x)$ , in the absence of gravity. The results are compared with the case of a system whose boundaries allow for mass flux (which we term 'open system' to indicate that mass in the chamber is not fixed), as was studied by Kodio et al [25] and Boyko et al [26]. These works have considered a system that includes a thin membrane on top of a liquid film, but coincide with the case of a free surface when bending effects are negligible [26]. The substantial difference in deformation at late

times between the closed and open system emphasizes the importance of the closed chamber for practical applications. Since in a real system it is impossible to apply a net zero force at the interface, and since the amplitude in such a system scales as  $\sim k^{-2}$  with the wavenumber,  $k$ , an open system may result in a dominant first mode “balloon shape” deformation even if the net force (the integral of the force distribution over the entire interface,  $\int_{-1}^1 f(x,t)dx$ ) is small. In contrast, for a closed system, mass conservation prevents the ‘ballooning’ effect even for strictly positive forcing and short waves can remain dominant even at steady-state.



In both the closed and open systems, the time scale to achieve a steady state will be governed by the first (slowest) eigenfunction. For the open system the first mode is a symmetric one with a time scale of  $\tilde{\tau} \cdot (2/\pi)^4$  and for the closed system, this is an asymmetric mode with a 5-fold faster time scale of  $\tilde{\tau} \cdot (1/2.4)^4$ .

FIG. 2. The effect of no-penetration conditions at the chamber boundaries on liquid film dynamics (all subfigures present half of the chamber, with a symmetry line at  $x=0$ ). (a) The external force distribution applied on the liquid-air interface along the chamber. (b) Comparison of the analytical solution for the case of impermeable boundaries (‘Closed chamber’, red dashed line) with the analytical solution for the case of permeable boundaries (‘Open chamber’, black dashed line), based on Boyko et al [26], at different times. At early times, the deformation exhibited by both systems is nearly identical. With time, deviations start evolving from the boundaries inward. Since in this case the force is strictly positive, the open system results in a continuous influx of liquid which ultimately leads to inflation of the interface to a ‘balloon’-like structure.

In contrast, the closed system, owing to its fixed mass, maintains short-wave deformations which follow the force distribution even at steady state, as shown in the inset of  $t=1$ . The solution presented for both systems is for the case of an initially flat interface and  $Bo=0$ .

**Experimental results.** To experimentally study the dynamics of thin film deformation, we used a 4 mm long, 8 mm wide and 50  $\mu\text{m}$  deep fluidic chamber (see Figure 1c) and filled it with a fixed volume of silicone oil (see material properties in the SI). The bottom of the chamber is patterned with an array of 200  $\mu\text{m}$  wide parallel electrodes, gapped by 200  $\mu\text{m}$  edge-to-edge. Upon application of a sinusoidal electric potential difference between the electrodes (500 Vpp, 10 kHz), the resulting localized electric field imposes dielectrophoretic (DEP) forces on the oil-air interface and deforms it. We used a digital holographic microscope [32] to observe the deformation of the interface in time. For each experiment we initially acquire the baseline surface topography prior to activation of the electric field, and then subtract it from all subsequent measurements. Figure 3 compares the experimental measurements with an analytical solution based on equation (0.3). The analytical solution is obtained using the force distribution presented in Figure 3a, corresponding to the DEP force on a liquid-air interface from

periodic electrodes [28]. Figures 3b-f present the evolution of the film in time, showing the gradual appearance of the different spatial modes. At very early times (0.2 ms) the highest spatial frequency is dominant, and the ‘tooth’-shaped peaks of the force distribution are also clearly observable in the analytical solution for the deformation. Experimental validation for these very early times and a detailed explanation for why they must be conducted as slightly different conditions is provided in [29]. At 2 ms, the model and the experimental measurements agree well and show that the 10<sup>th</sup> even mode of the system has grown significantly (note the change in scale from nm to  $\mu\text{m}$ ) and dominates the solution. The amplitude of the periodic deformation steadily increases, until at 37 ms a new qualitative change appears, initially in the form of a larger amplitude wave that penetrates from the boundaries. This is predicted well by the analytical model in good agreement with the experiments. By 3.55 s, the entire central region of the liquid has risen at the expense of the edges. The results continue to show good agreement, though some asymmetry begins to appear in the experimental measurements, resulting in slightly larger quantitative deviations. This is likely due to an additional low spatial frequency of the force distribution in the experiment that is not captured by the analytical force model and which therefore appears only at long times. At 100 s the system has achieved its steady state. The deformation at the center of the chamber is strictly positive. The overall shape and multitude of spatial frequencies is captured well by the theory, though quantitative differences, particularly on the right side of the chamber, are now evident.

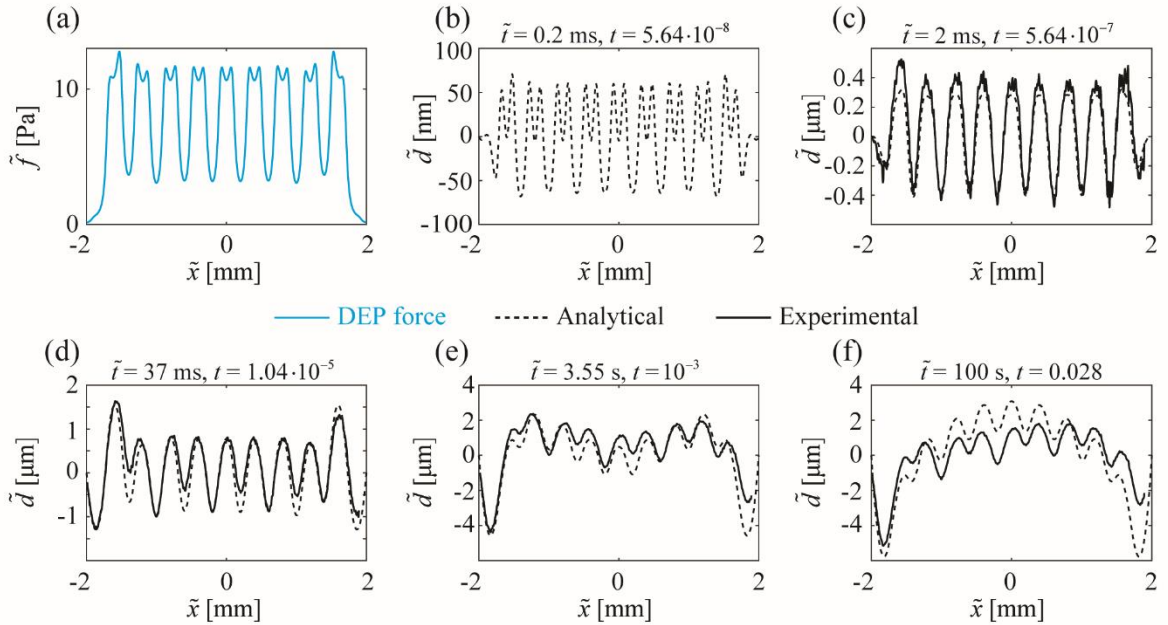


FIG 3. Validation of the analytical model against experimental measurements. (a) The DEP force distribution at the oil-air interface resulting from an array of parallel electrodes, as obtained from an electrostatic calculation in accordance with [28]. (b-f) The evolution of the film deformation from early times to steady state, showing the dominance of high wavenumbers at short times, and the gradual appearance of small wavenumbers with time. The analytical model successfully captures both the local and the global behavior of the film across multiple time scales. The chamber length is 4 mm, and is thus slightly truncated on the right the by 3.8 mm field of view of the holographic microscope. At the experiment we use silicone oil with kinematic viscosity of 200cSt and mass density of  $970 \text{ kg/m}^3$ . The complete parameters of the experiment are provided in the Supplementary Material [29].

*Concluding remarks.* Thin liquid films are found in endless applications such as spin coating, self-healing, and printing technologies, where infinite boundary conditions are appropriate for describing the film dynamics. However, there is an entire class of problems that inherently rely on no-penetration boundary conditions. For example, in liquid-based actuators, such as the ones used for adaptive optics [20], enclosed chambers with a fixed amount of liquid are naturally the most common implementation. Banerjee *et al.* have already shown the use of a membrane suspended over a thin liquid film as a mechanism for achieving freeform optical corrections with Zernike polynomials up to a 4<sup>th</sup> degree. However, the performance of such devices could not be predicted *a priori*, as no theory was available. The model we developed here provides insight into such systems and reveals the underlying eigenfunctions and their individual and collective dynamics. While our derivations focused on a free interface, they directly apply to the case of a membrane under dominant tension, and could also be readily extended to account for elastic bending. However, in order to quantitatively predict the response of actuation devices, the theory must be extended to two-dimensional domains.

In our derivation we focused on the case of normal forces applied directly to the liquid-air interface and implemented it using DEP. However, for other actuation mechanisms such as those that dictate a slip velocity (EOF) or an interface velocity (thermocapillary flow), the differential operator and the impermeability boundary conditions would be identical. The only thing that would differ is the RHS of equation (0.3) [33], but that would not change the solution procedure. When dictating a spatial force/velocity distribution in combination with the evolution equation, (0.1), care should be taken not to violate the underlying assumptions, at least not at the leading order of the solution; e.g. if dictating a slip velocity, then no-penetration at the domain boundaries would be fully satisfied under the lubrication approximation only if its magnitude and its spatial derivative vanish at the boundary.

Finally, we note that the non-self-adjointness is a manifestation of the mass conservation constraint on the system, and is likely to appear in other fluidic problems that are subjected to similar constraints, as well as in numerical solutions to such problems.

## References:

- [1] Lord Rayleigh, *LIX. On Convection Currents in a Horizontal Layer of Fluid, When the Higher Temperature Is on the under Side*, The London, Edinburgh, and Dublin Philosophical Magazine and Journal of Science **32**, 529 (1916).
- [2] H. Bénard, *Étude Expérimentale Des Courants de Convection Dans Une Nappe Liquide.—Régime Permanent: Tourbillons Cellulaires*, Journal de Physique Théorique et Appliquée **9**, 513 (1900).
- [3] J. H. Fink and R. W. Griffiths, *Radial Spreading of Viscous-Gravity Currents with Solidifying Crust*, J. Fluid Mech. **221**, 485 (1990).
- [4] I. J. Hewitt, N. J. Balmforth, and J. R. D. Bruyn, *Elastic-Plated Gravity Currents*, European Journal of Applied Mathematics **26**, 1 (2015).
- [5] J. E. Simpson, *Gravity Currents in the Laboratory, Atmosphere, and Ocean*, Annual Review of Fluid Mechanics **14**, 213 (1982).
- [6] J. B. Grotberg and O. E. Jensen, *Biofluid Mechanics in Flexible Tubes*, Annual Review of Fluid Mechanics **36**, 121 (2004).



- [7] K. O. McGraw and S. P. Wong, *Forming Inferences about Some Intraclass Correlation Coefficients.*, *Psychological Methods* **1**, 30 (1996).
- [8] A. Oron, S. H. Davis, and S. G. Bankoff, *Long-Scale Evolution of Thin Liquid Films*, *Rev. Mod. Phys.* **69**, 931 (1997).
- [9] Z. Zheng, M. A. Fontelos, S. Shin, and H. A. Stone, *Universality in the Nonlinear Leveling of Capillary Films*, *Phys. Rev. Fluids* **3**, 032001 (2018).
- [10] M. Backholm, M. Benzaquen, T. Salez, E. Raphaël, and K. Dalnoki-Veress, *Capillary Levelling of a Cylindrical Hole in a Viscous Film*, *Soft Matter* **10**, 2550 (2014).
- [11] R. V. Craster and O. K. Matar, *Dynamics and Stability of Thin Liquid Films*, *Rev. Mod. Phys.* **81**, 1131 (2009).
- [12] R. J. Deissler and A. Oron, *Stable Localized Patterns in Thin Liquid Films*, *Phys. Rev. Lett.* **68**, 2948 (1992).
- [13] B. Gjevik, *Occurrence of Finite-Amplitude Surface Waves on Falling Liquid Films*, *The Physics of Fluids* **13**, 1918 (1970).
- [14] D. J. Chappell and R. D. O’Dea, *Numerical-Asymptotic Models for the Manipulation of Viscous Films via Dielectrophoresis*, *Journal of Fluid Mechanics* **901**, (2020).
- [15] V. Frumkin and A. Oron, *Liquid Film Flow along a Substrate with an Asymmetric Topography Sustained by the Thermocapillary Effect*, *Physics of Fluids* **28**, 082107 (2016).
- [16] M. B. Williams and S. H. Davis, *Nonlinear Theory of Film Rupture*, *Journal of Colloid and Interface Science* **90**, 220 (1982).
- [17] Z. Zheng, M. A. Fontelos, S. Shin, M. C. Dallaston, D. Tseluiko, S. Kalliadasis, and H. A. Stone, *Healing Capillary Films*, *Journal of Fluid Mechanics* **838**, 404 (2018).
- [18] M. C. Dallaston, D. Tseluiko, Z. Zheng, M. A. Fontelos, and S. Kalliadasis, *Self-Similar Finite-Time Singularity Formation in Degenerate Parabolic Equations Arising in Thin-Film Flows*, *Nonlinearity* **30**, 2647 (2017).
- [19] C. V. Brown, G. G. Wells, M. I. Newton, and G. McHale, *Voltage-Programmable Liquid Optical Interface*, *Nature Photonics* **3**, 403 (2009).
- [20] K. Banerjee, P. Rajaeipour, Ç. Ataman, and H. Zappe, *Optofluidic Adaptive Optics*, *Appl. Opt.* **57**, 6338 (2018).
- [21] R. Eshel, V. Frumkin, M. Nice, O. Luria, B. Ferdman, N. Opatovski, K. Gommed, M. Shusteff, Y. Shechtman, and M. Bercovici, *Fabrication of Diffractive Optical Elements by Programmable Thermocapillary Shaping of Thin Liquid Films*, *ArXiv:2109.00158 [Physics]* (2021).
- [22] pengpeng zhao, D. Sauter, and H. Zappe, *Tunable Fluidic Lens with Dynamic High-Order Aberrationcontrol*, *Appl. Opt.* (2021).
- [23] F. Paratore, V. Bacheva, M. Bercovici, and G. V. Kaigala, *Reconfigurable Microfluidics*, *Nature Reviews Chemistry* **6**, 70 (2022).
- [24] A. E. Hosoi and L. Mahadevan, *Peeling, Healing, and Bursting in a Lubricated Elastic Sheet*, *Phys. Rev. Lett.* **93**, 137802 (2004).

- [25] O. Kodio, I. M. Griffiths, and D. Vella, *Lubricated Wrinkles: Imposed Constraints Affect the Dynamics of Wrinkle Coarsening*, Phys. Rev. Fluids **2**, 014202 (2017).
- [26] E. Boyko, R. Eshel, K. Gommed, A. D. Gat, and M. Bercovici, *Elastohydrodynamics of a Pre-Stretched Finite Elastic Sheet Lubricated by a Thin Viscous Film with Application to Microfluidic Soft Actuators*, Journal of Fluid Mechanics **862**, 732 (2019).
- [27] E. Boyko, D. Ilssar, M. Bercovici, and A. D. Gat, *Interfacial Instability of Thin Films in Soft Microfluidic Configurations Actuated by Electro-Osmotic Flow*, Phys. Rev. Fluids **5**, 104201 (2020).
- [28] I. Gabay, F. Paratore, E. Boyko, A. Ramos, A. D. Gat, and M. Bercovici, *Shaping Liquid Films by Dielectrophoresis*, Flow **1**, (2021).
- [29] *See Supplemental Material*, (n.d.).
- [30] L. G. Leal, *Advanced Transport Phenomena: Fluid Mechanics and Convective Transport Processes*. (Cambridge University Press, Leiden, 2007).
- [31] E. A. Coddington and N. Levinson, *Theory of Ordinary Differential Equations* (Tata McGraw-Hill Education, 1955).
- [32] E. Cuche, P. Marquet, and C. Depeursinge, *Simultaneous Amplitude-Contrast and Quantitative Phase-Contrast Microscopy by Numerical Reconstruction of Fresnel off-Axis Holograms*, Appl. Opt., AO **38**, 6994 (1999).
- [33] S. Rubin, A. Tulchinsky, A. D. Gat, and M. Bercovici, *Elastic Deformations Driven by Non-Uniform Lubrication Flows*, Journal of Fluid Mechanics **812**, 841 (2017).

## Supplementary Information

### **The non-self-adjoint thin film problem: dynamics of fixed-volume pinned films**

Israel Gabay<sup>1</sup>, Vesna Bacheva<sup>2</sup>, Dotan Ilssar<sup>3</sup>, Moran Bercovici<sup>1\*</sup>, Antonio Ramos<sup>4</sup>, Amir Gat<sup>1\*</sup>

<sup>1</sup>*Faculty of Mechanical Engineering, Technion – Israel Institute of Technology, Haifa, Israel*

<sup>2</sup>*IBM Research Europe, Zurich, Switzerland*

<sup>3</sup>*Department of Mechanical and Process Engineering, ETH Zürich, Zürich 8092, Switzerland*

<sup>4</sup>*Depto. Electronica y Electromagnetismo, Facultad de Fisica, Universidad de Sevilla, Sevilla, Spain*

*\*corresponding authors: M.B. ([mberco@technion.ac.il](mailto:mberco@technion.ac.il)) and A.G. ([amirgat@technion.ac.il](mailto:amirgat@technion.ac.il))*

## S1 – Detailed derivation of the analytic results

Figure 1 illustrates the examined configuration. A fluidic chamber with depth  $\tilde{h}_0$  and length  $\tilde{l}_c$  is filled with liquid with mass density  $\tilde{\rho}$ , and dynamic viscosity  $\tilde{\mu}$ . The liquid-air interface has a surface tension  $\tilde{\gamma}$  and is subjected to a normal force distribution  $\tilde{f}(\tilde{x}, \tilde{t})$ . The liquid velocities parallel and normal to the floor are  $\tilde{u}$  and  $\tilde{w}$  respectively and the liquid's pressure is  $\tilde{p}$ . We restrict our analysis to shallow geometries ( $\varepsilon = \tilde{h}_0 / \tilde{l}_c \ll 1$ ) with negligible inertia, i.e., small reduced Reynolds number ( $\text{Re}_r = \varepsilon^2 \tilde{U} \tilde{l}_c / \tilde{\nu} \ll 1$ ), where  $\tilde{U}$  is the characteristic velocity along the chamber and  $\tilde{\nu} = \tilde{\mu} / \tilde{\rho}$  is the kinematic viscosity of the liquid. Under those assumptions, we obtain the following lubrication equations for two-dimensional system,

$$(1.1) \quad \frac{\partial \tilde{u}}{\partial \tilde{x}} + \frac{\partial \tilde{w}}{\partial \tilde{z}} = 0, \quad \frac{\partial \tilde{p}}{\partial \tilde{x}} = \tilde{\mu} \frac{\partial^2 \tilde{u}}{\partial \tilde{z}^2}, \quad \frac{\partial \tilde{p}}{\partial \tilde{z}} = -\tilde{\rho} \tilde{g}.$$

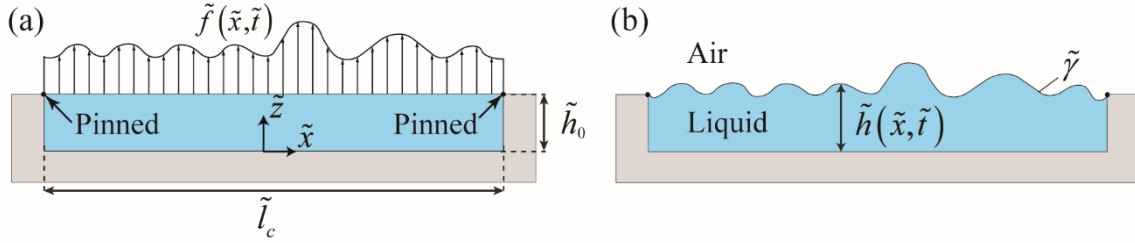


**FIG S.1.** An illustration of the investigated configuration. A shallow fluidic chamber of length  $\tilde{l}_c$  and height  $\tilde{h}_0$  filled with a liquid with mass density  $\tilde{\rho}$  and dynamic viscosity  $\tilde{\mu}$ , is open to the air above. (a) The liquid-air interface is subjected to a normal force distribution  $\tilde{f}(\tilde{x}, \tilde{t})$ , and has a surface tension  $\tilde{\gamma}$ . (b) Upon activation, the normal force at the interface deforms the liquid film. We denote the film height as  $\tilde{h}(\tilde{x}, \tilde{t})$ . The liquid is pinned at the edges of the chamber.

The velocity boundary conditions on the bottom (rigid) surface are  $(\tilde{u}, \tilde{w})|_{\tilde{z}=0} = (0, 0)$ , corresponding to no penetration and no-slip conditions. The boundary conditions at the liquid-air interface include the kinematic boundary condition, which relates the liquid velocities at the interface with its deformations, and a stress balance on the interface (the dynamic boundary condition). We here consider a system without external tangential forces, nor variation in surface tension along the interface. Thus, the boundary conditions are,

$$(1.2) \quad \begin{cases} (\tilde{u}, \tilde{w}) = (0, 0) & \text{at } \tilde{z} = 0 \\ \left\{ \begin{array}{l} \tilde{w} = \partial \tilde{h} / \partial \tilde{t} + \tilde{u} \cdot \partial \tilde{h} / \partial \tilde{x} \\ \tilde{p} = \tilde{p}_a - \tilde{\gamma} \frac{\partial^2 \tilde{h}}{\partial \tilde{x}^2} - \tilde{f}(\tilde{x}, \tilde{t}) \\ \partial \tilde{u} / \partial \tilde{z} = 0 \end{array} \right. & \text{at } \tilde{z} = \tilde{h}(\tilde{x}, \tilde{t}), \end{cases}$$

note that the conditions on the liquid-air interface are linearized under the long wave approximation. The solution of the momentum equation parallel to the floor yields the Poiseuille flow profile,

$$(1.3) \quad \tilde{u} = \frac{\partial \tilde{p}}{\partial \tilde{x}} \frac{1}{2\tilde{\mu}} \left( \frac{\tilde{z}^2}{\tilde{h}^2} - 2 \frac{\tilde{z}}{\tilde{h}} \right).$$

By integrating the continuity equation with respect to  $\tilde{z}$  and substituting equation (1.3) and boundary conditions (1.2), we obtain the well-known thin film equation,

$$(1.4) \quad \frac{\partial \tilde{h}}{\partial \tilde{t}} = \frac{1}{3\tilde{\mu}} \frac{\partial}{\partial \tilde{x}} \left( \tilde{h}^3 \frac{\partial \tilde{p}}{\partial \tilde{x}} \right).$$

To find the liquid's pressure as a function of  $\tilde{h}$ , we solve the  $\tilde{z}$ -direction of the momentum equation. Using the normal dynamic boundary condition, we obtain,

$$(1.5) \quad \tilde{p} = \tilde{p}_a + \tilde{\rho}\tilde{g}(\tilde{h} - \tilde{z}) - \tilde{\gamma} \frac{\partial^2 \tilde{h}}{\partial \tilde{x}^2} - \tilde{f}.$$

Substituting the pressure (1.5) into (1.4) yields the relevant evolution equation,

$$(1.6) \quad \frac{\partial \tilde{h}}{\partial \tilde{t}} = \frac{1}{3\tilde{\mu}} \frac{\partial}{\partial \tilde{x}} \left( \tilde{h}^3 \left( \tilde{\rho}\tilde{g} \frac{\partial \tilde{h}}{\partial \tilde{x}} - \tilde{\gamma} \frac{\partial^3 \tilde{h}}{\partial \tilde{x}^3} - \frac{\partial \tilde{f}}{\partial \tilde{x}} \right) \right).$$

As shown in figure 1, we examine a closed chamber with rigid walls at the boundaries. Due to the chamber geometry, we require pinning of the film at the chamber edges,  $\tilde{h} = \tilde{h}_0$ . In addition, modeling a closed chamber requires that  $\tilde{u} = 0$  at the boundaries. Integrating the momentum equation in the  $\tilde{z}$  direction, and requiring no penetration at the edges, yields  $\partial \tilde{p} / \partial \tilde{x} = 0$ . Applying this requirement to (1.2) translates to the following conditions on the film height,

$$(1.7) \quad \tilde{h} = \tilde{h}_0, \quad \tilde{\rho}\tilde{g} \frac{\partial \tilde{h}}{\partial \tilde{x}} - \tilde{\gamma} \frac{\partial^3 \tilde{h}}{\partial \tilde{x}^3} - \frac{\partial \tilde{f}}{\partial \tilde{x}} = 0, \quad \text{at } x = \pm 1 \text{ and } t \geq 0.$$

These boundary conditions are accompanied by an initial condition,  $\tilde{h}(\tilde{x}, t = 0) = \tilde{h}_i(\tilde{x})$ .

Using the following non-dimensional parameters  $\tilde{t} = t\tilde{\tau}$ ,  $\tilde{x} = x\frac{\tilde{l}_c}{2}$ ,  $\tilde{h} = h\tilde{h}_0$ ,  $\tilde{f} = \tilde{F}f$  and assuming small deformation with respect to the chamber height (the height of the fluid at the edges,  $\tilde{h}_0$ ),  $\tilde{d} \ll \tilde{h}_0$ , we obtain the non-dimensional linear equation for the film deformation,

$$(1.8) \quad d_t + d_{xxx} - \text{Bo}d_{xx} = -\Pi f_{xx},$$

where the deformations defined as,  $d(x, t) = 1 - h(x, t)$ . The subscripts  $x$  and  $t$  represent derivative with respect to  $x$  and  $t$  respectively.  $\text{Bo} = \frac{\tilde{\rho}\tilde{g}\tilde{l}_c^2}{4\tilde{\gamma}}$  is the Bond number,  $\Pi = \frac{\tilde{F}\tilde{l}_c^2}{4\tilde{\gamma}\tilde{h}_0}$  represents the balance between the force distribution at the interface versus the surface tension, and the characteristic time-scale is  $\tilde{\tau} = \frac{3\tilde{\mu}\tilde{l}_c^4}{16\tilde{h}_0^3\tilde{\gamma}}$ . The resulting non-dimensional boundary conditions for the deformation are,

$$(1.9) \quad d = 0, \quad d_{xxx} - \text{Bo} \cdot d_x = -\Pi f_x \quad \text{at } x = \pm 1 \text{ and } t \geq 0,$$

This set of boundary conditions generate a non-self-adjoint system. To observe this, we first homogenize the boundary conditions by defining the deformation as  $d(x, t) = \hat{d}(x, t) + P(x)\theta(t)$ , where  $P(x)$  is a polynomial function that we determined according to the force distribution at the chamber edges. We

furthermore assume that the normal force distribution applied instantaneously upon activation of the electric field, and thus

$$(1.10) \quad \hat{d}_t + \hat{d}_{xxx} - \text{Bo} \cdot \hat{d}_{xx} = -\Pi\theta(t)f_{xx} - P\delta(t) + \text{Bo}P_{xx}(x)\theta(t),$$

and,

$$(1.11) \quad P(x,t) = \Pi \frac{f_x(x=1) - f_x(x=-1)}{4\text{Bo}} (x^2 - 1) + \Pi \frac{f_x(x=1) + f_x(x=-1)}{4(\text{Bo} - 3)} (x^3 - x),$$

where  $\theta(t)$  and  $\delta(t)$  are the Heaviside step function and the Dirac delta function respectively. We note that this polynomial homogenises the boundary conditions for any Bond number excepts  $\text{Bo} = 0, 3$ , which is undefined. To cover these two specific cases, one needs to work with a one degree higher of polynomial function. Now we yield a new system of equations and boundary conditions where the source term has been changed as can be seen in (1.10). However, the boundary conditions now are homogenous,

$$(1.12) \quad \begin{aligned} \hat{d}(x = \pm 1, t) &= 0 \\ \hat{d}_{xxx}(x = \pm 1, t) - \text{Bo} \cdot \hat{d}_x(x = \pm 1, t) &= 0. \\ \hat{d}(x, t = 0) &= d_i \end{aligned}$$

The resulting PDE and boundary conditions for  $\hat{d}(x,t)$  yield a non-self-adjoint system as explained later in the text. To solve this system, we use the generalized form of the separation of variables method [1]. Assuming the standard form of solution,

$$(1.13) \quad \hat{d}(x,t) = \sum_{n=0}^{\infty} X_n(x)T_n(t),$$

where  $X$  depends solely on the spatial coordinate,  $x$ , and  $T$  is a time dependent function. Substituting (1.13) to the homogenous form of equation (1.10), yields two sperate equations,

$$(1.14) \quad -\frac{T'}{T} = \frac{X^{(4)}}{X} - \text{Bo} \frac{X''}{X} = \lambda^4.$$

For a 1D functions (such as  $X$  and  $T$ ) we denote the function derivative with  $X'$  and  $X^{(n)}$  representing the n-th derivative order of the function  $X$ . The boundary conditions for the spatial function,  $X$  are,

$$(1.15) \quad X(\pm 1) = 0, \quad X'''(\pm 1) - \text{Bo} \cdot X'(\pm 1) = 0.$$

For  $\lambda_0 = 0$ , the eigenfunction is,

$$(1.16) \quad X_0 = \frac{\sqrt{\text{Bo}} \left( \cosh(\sqrt{\text{Bo}}x) - \cosh(\sqrt{\text{Bo}}) \right)}{2 \left( \sinh(\sqrt{\text{Bo}}) - \sqrt{\text{Bo}} \cosh(\sqrt{\text{Bo}}) \right)},$$

and the rest of the eigenfunctions of the system are,

$$(1.17) \quad X_n = \begin{cases} \sin(\alpha_n x) - \frac{\sin(\alpha_n)}{\sinh(\beta_n)} \sinh(\beta_n x) & \text{for odd n numbers} \\ \cos(\alpha_n x) - \frac{\cos(\alpha_n)}{\cosh(\beta_n)} \cosh(\beta_n x) & \text{for even n numbers} \end{cases},$$

where  $\alpha_n = \sqrt{\frac{-Bo + \sqrt{Bo^2 + 4\lambda_n^4}}{2}}$ , and  $\beta_n = \sqrt{\frac{Bo + \sqrt{Bo^2 + 4\lambda_n^4}}{2}}$  are functions of the Bond number. The eigenvalues are calculated from the following two transcendental equations, one for each set of eigenfunctions presented at (1.17),

$$(1.18) \quad \begin{cases} \alpha \sin(\alpha) = -\beta \cos(\alpha) \tanh(\beta) \\ \beta \sin(\alpha) = \alpha \cos(\alpha) \tanh(\beta) \end{cases}.$$

The zero eigenfunction is the only one that has a non-zero integral over the domain. Meaning that, for any amount of liquid that is not equal to the chamber's volume, the zero eigenfunction will determine the film shape for  $f(x,t) = 0$ .

One of the consequences of a non-self-adjoint system is that the obtained sets of eigenfunctions aren't orthogonal to themselves. Thus, to solve for the film deformation we need to find a set of orthogonal functions to the original eigenfunctions. To achieve that, we first derive the Lagrange adjoint operator,  $L^+$ , i.e., the adjoint equation. In our case, due to the simplicity of the equation (linear, consisting of only even derivatives with real and constant coefficients), the adjoint operator is the same differential operator,  $L$ , just with different boundary conditions. To derive the boundary conditions of the adjoint equation we require  $\langle L[X], Y \rangle = \langle X, L^+[Y] \rangle$ , where  $\langle U, V \rangle = \int_{-1}^1 U V dx$  is the basic inner product. Applying the inner product relation, integrating by parts and substituting the boundary conditions, (1.15), yields,

$$(1.19) \quad [X''Y' + XY''']_{-1}^1 = 0.$$

Thus, the resulting adjoint system is

$$(1.20) \quad \begin{aligned} \frac{Y^{(4)}}{Y} - Bo \frac{Y''}{Y} &= \lambda_n^4 \\ Y'(\pm 1) &= Y''(\pm 1) = 0 \end{aligned}.$$

For  $\lambda_0 = 0$ , the resulting eigenfunction is  $Y_0 = Const$ , and the rest of the eigenfunctions of the adjoint system are,

$$(1.21) \quad Y_n = \begin{cases} \sin(\alpha_n x) - \frac{\alpha_n \cos(\alpha_n)}{\beta_n \cosh(\beta_n)} \sinh(\beta_n x) & \text{for odd } n \text{ numbers} \\ \cos(\alpha_n x) + \frac{\alpha_n \sin(\alpha_n)}{\beta_n \sinh(\beta_n)} \cosh(\beta_n x) & \text{for even } n \text{ numbers} \end{cases}.$$

The transcendental equations for each (odd and even  $n$ ) eigenvalues are the same as for the original system, and thus the eigenvalues are unchanged. Using the orthogonal base (1.17) we present the close form solution for  $\hat{d}(x,t)$  by the solution of (1.10),

$$(1.22) \quad T_n' X_n + \lambda_n^4 X_n T_n = (-\Pi f_{xx}(x) + Bo \cdot P_{xx}) \theta(t) - P(x) \delta(t).$$

The solution of (1.22) is,

$$(1.23) \quad T_n(t) = \theta(t) \left[ \frac{a_n (1 - \exp(-\lambda_n^4 t))}{\lambda_n^4} - b_n \exp(-\lambda_n^4 t) \right] + \exp(-\lambda_n^4 t) (b_n \theta(0) + I_n),$$

where  $a_n, b_n, I_n$  are the coefficients of the generalized Fourier series of the following functions,  $-\Pi f_{xx}(x) + \text{Bo} P_{xx}(x), P(x), d_i(x)$  respectively. For a non-self-adjoint system, these coefficients can be found through the orthogonality of the eigenfunctions of the original and the adjoint systems. In practice, for a general function  $g(x)$  the series expansion by the system eigenfunctions is,

$$(1.24) \quad g(x) = \sum_{n=0}^{\infty} c_n X_n(x); \quad c_n = \frac{\int_{-1}^1 g(x) Y_n dx}{\int_{-1}^1 X_n Y_n dx}.$$

We note that the solution, (1.23), was solved for the case of  $a_0 = 0$ . For non-zero  $a_0$ , one should obtain an extra term which is a linear function of  $t$ . This is not a physical behavior of our system cause the zero eigenfunction has a non-zero volume, i.e., non-zero integral over the domain. This will create an effect of a linear decreasing or increasing volume effect with time which obviously is not physical in a mass conservative system. For consistency we show that  $a_0 = 0$  for any force distribution,

$$(1.25) \quad a_0 = \frac{\int_{-1}^1 (-\Pi f_{xx} + \text{Bo} \cdot P_{xx}) Y_0 dx}{\int_{-1}^1 X_0 Y_0 dx} = \int_{-1}^1 (-\Pi f_{xx} + \text{Bo} \cdot P_{xx}) dx = 0.$$

$Y_0 = \text{const}$ , so we can take it out of the integral and by substituting  $P(x)$ , (1.11), we yield  $a_0 = 0$ . With that, the solution for the deformation of the film can be written as,

$$(1.26) \quad d(x,t) = P(x)\theta(t) + \sum_{n=0}^{\infty} X_n(x) T_n(t).$$

The solution methodology is very similar to the regular separation of variable method for self-adjoint system. Where the main difference is that we here need to solve for two system which due to the non-self-adjointness are different in order to be able to expand the source terms and initial condition in terms of the eigenfunction of the system. After we have that the rest is straightforward.



## S2 – Open chamber solution

A comparison with the case of open boundaries is required in order to understand the effect of closed boundary conditions. We thus present here the solution for the open case, which is governed by a self-adjoint thin film problem. For simplicity, we consider a system with negligible gravity ( $Bo=0$ ), and zero force gradient at the chamber edges. Figure 2 presents the closed and open cases. For the closed chamber the no penetration condition is applied as zero third derivative of the deformation,  $d_{xxx}(x=\pm 1, t)=0$ , while for the open chamber, the free in- or out-flow of liquid through the edge is applied by the second derivative of the deformation,  $d_{xx}(x=\pm 1, t)=0$ , as presented by Boyko et al. [2].

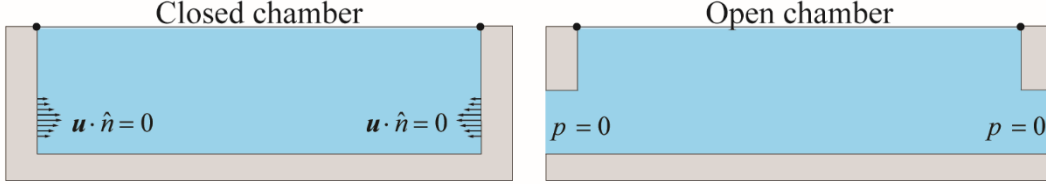


**FIG S.2.** Illustration of the two system we consider. At the left, the closed chamber case which we consider and solved in this work, and from the right the Open chamber case, where fluid can flow in or out through the chamber edges.

$$d_t + d_{xxxx} = -\Pi f_{xx}$$

We assume that the fluid is initially at rest, i.e.  $d(x, t=0) = 0$  and that the fluid pressure is zero at the edges [3], i.e. the sidewalls of the chamber are open and connected to big reservoirs such that fluid can flow in and out. The boundary conditions are,

$$(2.1) \quad d = 0, \quad \frac{\partial^2 d}{\partial x^2} = 0, \quad \text{at } x = \pm 1 \text{ and } t \geq 0.$$

The general solution can be obtained by using the Green function [4] for this equation using such homogenous boundary conditions is given by

$$(2.2) \quad d(x, t) = \int_0^2 d_i(\xi) G(x, \xi, t) d\xi + \int_0^t \int_0^2 \Phi(\xi, \tau) G(x, \xi, t - \tau) d\xi d\tau.$$

$d_i$  is the initial deformation which, in our case is zero, so the left integral vanishes.  $\Phi$  is the source term of the equation which in our case is  $\Phi(x, t) = -\Pi f_{xx}$ , and the Green function is given by

$$(2.3) \quad G(x, \xi, t) = \sum_{m=1}^{\infty} \sin(\lambda_m x) \sin(\lambda_m \xi) \exp(-\lambda_m^4 t),$$

where the eigen values of the system are,  $\lambda_m = \frac{\pi}{2} m$ .

We note that this Green function is given for a finite domain  $0 \leq x \leq l$ . Hereafter, for simplicity, we set  $l=2$  yielding to

$$(2.4) \quad d(x, t) = \sum_{m=1}^{\infty} \sin(\lambda_m x) \int_0^t \int_0^2 (\sin(\lambda_m \xi) \Phi(\xi, \tau)) \exp(-\lambda_m^4 (t - \tau)) d\xi d\tau$$

$$d(x, t) = \sum_{m=1}^{\infty} \sin(\lambda_m x) \frac{1 - \exp(-\lambda_m^4 t)}{\lambda_m^4} \int_0^2 (\sin(\lambda_m \xi) \Phi(\xi, \tau)) d\xi$$

### S3 – Device fabrication & the experimental setup

#### Device fabrication

FIG S.3. illustrates the device configuration and its fabrication process. We create the electrodes by a lift-off process using a 2 nm thick Pt layer sandwiched between two 2 nm thick Ti layers on a borosilicate wafer. To create the fluidic chamber, we patterned a 50  $\mu\text{m}$  thick layer of SU-8 photoresist on top of the wafer. Finally, we diced the wafer to separate individual devices. The microfluidic chamber we used in the experiments is 4 mm wide and 8 mm long and contains at its floor an interdigitated electrode configuration with 200  $\mu\text{m}$  wide electrodes, gapped by 200  $\mu\text{m}$  edge to edge.

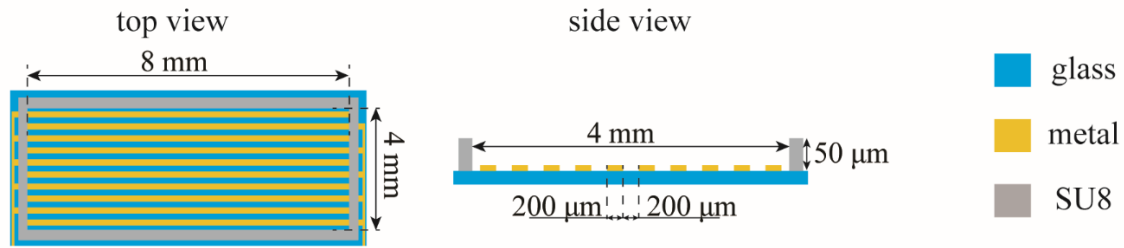


**FIG S.3.** Illustration of the device used in the experiments, consisting of a microfluidic chamber defined by 50  $\mu\text{m}$  tall SU8 walls and containing an array of 200  $\mu\text{m}$  wide interdigitated electrodes at its bottom.

#### Experimental setup

FIG S.4. presents schematics of the experimental setup. The device is mounted on a home-made connector composed of 3D printed housing and a printed circuit board (PCB) containing electric pins interfacing the device with a voltage amplifier (2210-CE, TREK), which amplifies the voltage output of a wave generator (TG5012A, AIM-TTI Instruments). The device is placed under a digital holographic microscope (DHM R1000, Lyncee tec) allowing observation of the oil-air interface by recording a hologram image on a digital sensor and using a numerical algorithm for real-time reconstruction.

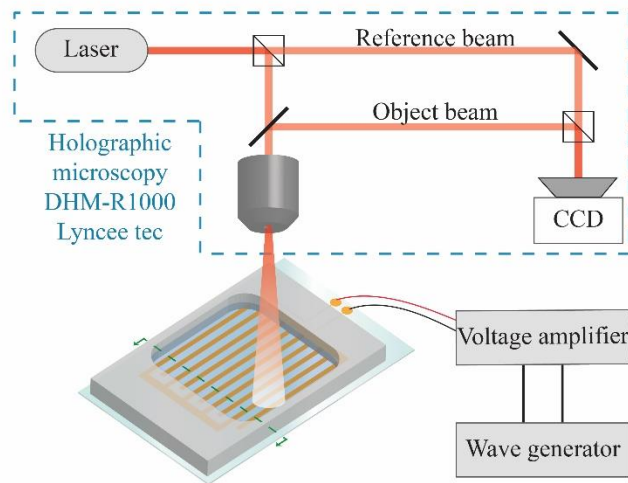


**FIG S.4.** Schematics of the experimental setup. The device is connected to a voltage amplifier, which amplifies a sinusoidal AC signal supplied by a wave generator. We use a digital holographic microscope to observe the deformation of the oil-air interface when subjected to an electric field.

## **Experimental conditions**

### *Main text*

The experimental data presented in the main text was recorded with a 1.25X objective with a field of view of 3.8X3.8 mm<sup>2</sup>. The silicone oil placed in the chamber has mass density of  $\tilde{\rho}=970\text{kg/m}^3$ , kinematic viscosity of  $\tilde{\nu}=200\text{cSt}$ , surface tension of  $\tilde{\gamma}=21\cdot 10^{-3}\text{N/m}$  and electric permittivity of  $\tilde{\epsilon}=2.7\tilde{\epsilon}_0$ , where  $\tilde{\epsilon}_0$  is the permittivity of free space. The voltage difference between the electrodes was a sinusoidal wave with 500 Vpp and a frequency of 10 kHz.

### *Supplemental Material (Section S.4)*

The experimental data presented in the next chapter was recorded with a 2.5X objective with a field of view of 1.9X1.9 mm<sup>2</sup>. The silicone oil placed in the chamber has a mass density of  $\tilde{\rho}=970\text{kg/m}^3$ , kinematic viscosity of  $\tilde{\nu}=1000\text{cSt}$ , surface tension of  $\tilde{\gamma}=21\cdot 10^{-3}\text{N/m}$  and electric permittivity of  $\tilde{\epsilon}=2.7\tilde{\epsilon}_0$ , where  $\tilde{\epsilon}_0$  is the permittivity of free space. The voltage difference between the electrodes was a sinusoidal wave with 500 Vpp and a frequency of 10 kHz.

#### S4 – Experimental measurements of early times

In Figure 3 of the main manuscript, we did not present the experimental results for very early times ( $0.2 \text{ ms}$ ,  $5 \cdot 10^{-8}$  in non-dimensional time), as those were too short for the imaging system to capture. Thus, to capture early times, we performed another experiment with more viscous silicone oil (1000 cSt compared to 200 cSt in the manuscript) and also placed less volume of liquid in the chamber resulted in thinner film. Both actions increase the hydrodynamic resistance of the system and resulted in larger time scale,  $\tilde{\tau} = 3\tilde{\mu}\tilde{l}^4 / 16\tilde{h}_0^3\tilde{\gamma}$ . We note that, despite the small liquid volume, the liquid is still pinned at the edges of the chamber, resulting in initial conditions of a bowl shape film that is  $50 \mu\text{m}$  in height at the edges and approximately  $20 \mu\text{m}$  in height at the chamber's center. We compare the experimental measurements with an analytical solution where we assume a film with a uniform height of  $30 \mu\text{m}$ , corresponding to the average film thickness in the chambers. Due to this difference, we expect only a qualitative comparison between the two.

Figure S.5(a) shows the force distribution due to the array of electrodes. The force distribution is characterized by ‘tooth’-shaped peaks that contain the smallest wavelength in the system, resulting from the transition region between adjacent electrodes. As shown by equations (1.17), and (1.23), large spatial wavenumbers are associated with a rapid temporal response and in order to isolate them we must turn to short times. Figure S.5.b-f presents the deformation of the film at different times under the interfacial force distribution as shown in subfigure S.5.a. At 2 ms only the highest spatial frequency, is visible, in good agreement with the analytical prediction. At 22 ms a longer wavelength is already clearly visible and as time continues becomes the dominant feature of the deformation.

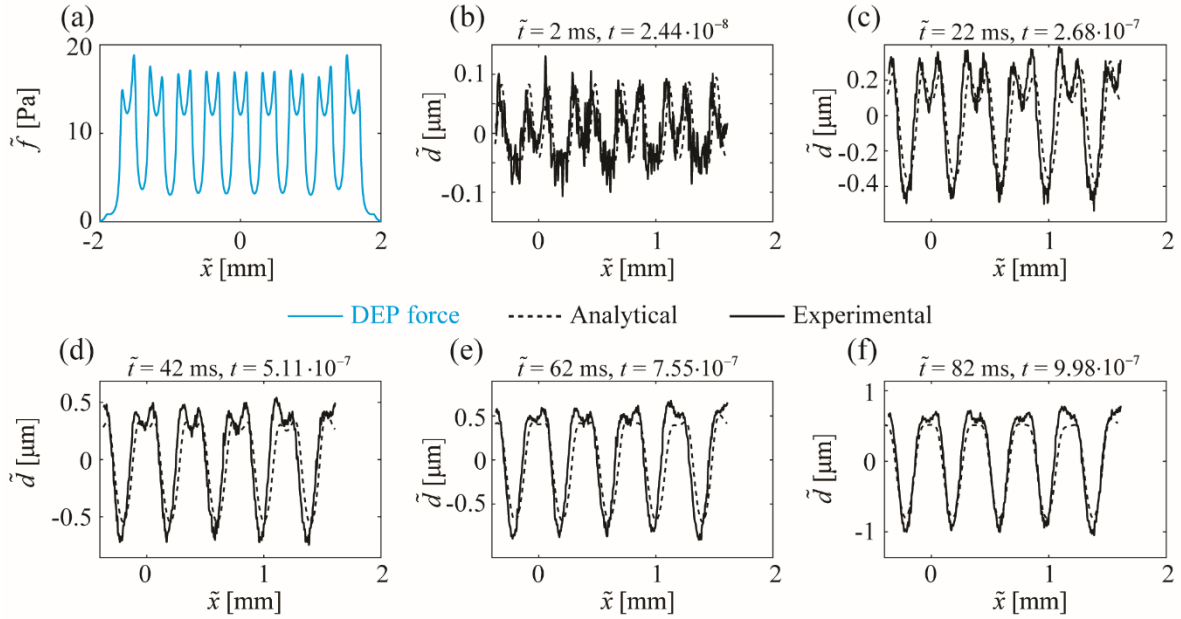


**FIG. S.5.** Validation of the analytical model with experimental measurements at very small non-dimensional times,  $t < 10^{-6}$ . (a) DEP force distribution at the oil air interface of a  $30 \mu\text{m}$  film, as obtained from electrostatic calculations [5]. (b-f) Comparison between the analytical solution (black dashed line) and the experimental measurements (black solid line) of the film deformations at different times. At short times the ‘tooth’-shaped peaks, corresponding to the highest spatial frequency, dominate the deformation. At later times, additional lower frequencies appear and overtake the higher frequencies in amplitude. In this experiment we use silicone oil with kinematic viscosity of 1000 cSt and mass density of  $970 \text{ kg/m}^3$ .

## References

- [1] E. A. Coddington and N. Levinson, *Theory of Ordinary Differential Equations* (Tata McGraw-Hill Education, 1955).
- [2] E. Boyko, R. Eshel, K. Gomed, A. D. Gat, and M. Bercovici, *Elastohydrodynamics of a Pre-Stretched Finite Elastic Sheet Lubricated by a Thin Viscous Film with Application to Microfluidic Soft Actuators*, *Journal of Fluid Mechanics* **862**, 732 (2019).
- [3] O. Kodio, I. M. Griffiths, and D. Vella, *Lubricated Wrinkles: Imposed Constraints Affect the Dynamics of Wrinkle Coarsening*, *Phys. Rev. Fluids* **2**, 014202 (2017).
- [4] A. D. Polianin, *Handbook of Linear Partial Differential Equations for Engineers and Scientists* (Chapman & Hall/CRC, Boca Raton, 2002).
- [5] I. Gabay, F. Paratore, E. Boyko, A. Ramos, A. D. Gat, and M. Bercovici, *Shaping Liquid Films by Dielectrophoresis*, *Flow* **1**, (2021).